Gas-Phase Hydroxyl Radical Generation by the Surface Reactions over Basic Metal Oxides

ARTICLE *in* THE JOURNAL OF PHYSICAL CHEMISTRY B · APRIL 1998

Impact Factor: 3.3 · DOI: 10.1021/jp9731314

4 AUTHORS, INCLUDING:

Suguru Noda
Waseda University
91 PUBLICATIONS **1,477** CITATIONS
SEE PROFILE

Azuchi Harano
Gunma University
20 PUBLICATIONS **292** CITATIONS
SEE PROFILE

Gas-Phase Hydroxyl Radical Generation by the Surface Reactions over Basic Metal Oxides

Suguru Noda,*,† Masateru Nishioka,† Azuchi Harano,‡ and Masayoshi Sadakata†

Department of Chemical System Engineering, Graduate School of Engineering, The University of Tokyo, 7-3-1, Hongo, Bunkyo-ku, Tokyo 113-8656, Japan, and Department of Biological and Chemical Engineering, Faculty of Engineering, Gunma University, 1-5-1 Tenjin-Cho, Kiryu, Gunma-ken, 376-8515, Japan

Received: September 26, 1997; In Final Form: December 31, 1997

Hydroxyl radical desorption in the heterogeneous catalytic reactions of water or hydrogen with oxygen was examined by laser-induced fluorescence spectroscopy. The catalytic activities of Pt, Al_2O_3, and basic metal oxides (MgO, CaO, SrO, BaO) supported on Al_2O_3 were studied in the pressure range 0.1−10 Torr and the temperature range 1100−1300 K. In the case of OH generation from water, the catalytic activities of Pt and all oxides except Al_2O_3 were very high and the OH concentration reached the equilibrium value within a residence time of 4 ms. In the case of hydrogen oxidation, differences in the catalytic behavior were clearly observed. The surface reaction mechanisms and the effects of Al_2O_3 and MgO on gas-phase ignition are discussed.

Introduction

Gas-phase OH radicals are strong oxidizing agents and known to be important chain carriers in combustion, so they are expected to act as promoters in some reactions such as catalytic combustion.[1] To date, much research has been performed on the OH desorption in heterogeneous catalyzed reactions over the surfaces of noble metals. Ljungström et al. studied the catalytic activities of several metals, and they found that the order of the catalytic activities of the metals was Pt > Pd > Rh > Ir > Ni.[2] Pt is the most frequently studied catalyst, and the kinetics of catalyzed reactions on its surface were explained by a simulation incorporating a series of reactions among the neutral species.[3−6] On the other hand, only a few studies have been performed on the OH desorption from metal oxides. The reactions of methane or water with oxygen over basic lanthanide oxides were examined by Lunsford's group.[7,8] The more basic oxide proved to have the higher activity (La_2O_3 > Nd_2O_3 > Sm_2O_3 > MgO > Yb_2O_3 > CeO_2) for OH generation, and reactions containing ionic species were proposed.

Thermodynamically, there are two strategies to produce OH by heterogeneous catalytic reaction. One is to produce OH below the thermodynamic equilibrium concentration from species that have low chemical potential only by applying heat. The other is to produce OH at a high concentration by applying heat to species that have high chemical potential. In this work, OH generation was examined in the catalytic reactions of water (which has low chemical potential) or hydrogen (which has high chemical potential) with oxygen by laser-induced fluorescence (LIF) spectroscopy. We examine the catalytic properties of Pt, basic metal oxides (MgO, CaO, SrO, BaO), and Al_2O_3 and discuss the mechanisms governing OH generation.

Experimental Section

LIF System. The LIF measurement system is shown in Figure 1. Briefly, the second harmonic of the dye laser (rhodamine 590, pumped by a Q-switched Nd:YAG laser) was used for OH−LIF. The OH was excited by the $A^2\Sigma^+(v' = 1) \leftarrow X^2\Pi(v = 0)$ $Q_1(4)$ transition at 282.44 nm. The change of the amplitude of this transition relative to the total amplitude is insignificant in the temperature range of our experiments.[8] The fluorescence of the $A^2\Sigma^+(v' = 1) \rightarrow X^2\Pi(v'' = 1)$ transition around 314 nm was collected on a photomultiplier tube equipped with two quartz glass lenses, a band-pass filter (313 nm, bandwidth of 10 nm), and a slit set vertically with respect to the laser beam. The signal was amplified, accumulated by a boxcar integrator, and transferred to a computer. The time decay of the LIF was also observed by a digital oscilloscope to estimate the collisional quenching.

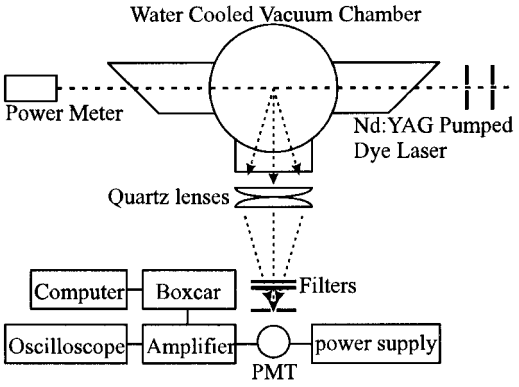

Figure 1. Schematic diagram of the LIF system.

OH Measurement under Thermodynamic Equilibrium Conditions. First, we measured the OH concentration under thermodynamic equilibrium conditions to derive the absolute OH concentration from the LIF signal. OH was generated by heating a gas mixture of H_2O, O_2, and Ar in the reaction cell. The cell was composed of a quartz glass tube with a heating line, a thermocouple, and fire bricks as shown in Figure 2. Pure oxygen, argon, and water-saturated argon were mixed at atmospheric pressure. The gas mixture was supplied to the quartz glass tube and pumped out by a rotary pump with a liquid

* To whom correspondence should be addressed. Telephone: +81-3-5802-8996. Fax: +81-3-5802-2997. E-mail: snoda@env-lab.t.u-tokyo.ac.jp.
† The University of Tokyo.
‡ Gunma University.

S1089-5647(97)03131-3 CCC: $15.00
Published on Web 04/02/1998

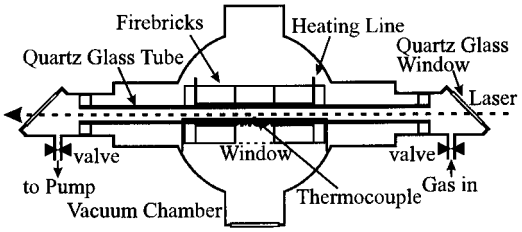

Figure 2. Top view of the experimental apparatus for OH measurement under the thermal equilibrium conditions.

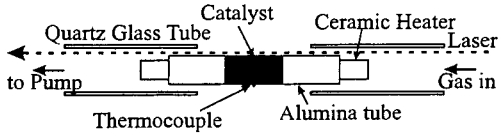

Figure 3. Side view of the flow tube reactor for the catalytic OH generation.

nitrogen trap. Thermodynamic equilibrium conditions were obtained when the valves on both sides of the tube were closed. OH was excited by the laser, and the fluorescence was observed through the window in the firebrick. From the lifetime of the OH−LIF, the quenching rate constant of each gas was obtained. These rate constants were used to derive the absolute concentration from the LIF signals in this and the following experiments.

Catalytic Generation of OH over the Surfaces. The flow tube reactor for the catalytic generation of OH is shown in Figure 3. It was composed of two quartz glass tubes and a SiC ceramic heater covered with three alumina tubes. A K-type thermocouple was put on the surface of the middle alumina tube and covered with alumina paste, and the catalyst was supported on it. For the basic metal oxides, a specific amount (3 mL) of an aqueous solution of nitrate (0.1 M) was painted on the middle alumina tube and dried in the atmosphere at about 420 K. Then the nitrates were heated and kept at 1300 K for an hour under a 20% O_2/Ar flow at 6 Torr where they were decomposed into oxides. In the case of Pt, platinum paste was painted and calcined at 1300 K for an hour in the atmosphere. Reactant gas was supplied to the reactor and pumped out by a rotary pump with a liquid nitrogen trap. The desorbed OH was measured 2 mm above the catalyst. Standard conditions for the experiment were 1200 K, 6.0 Torr, and a 4 ms residence time.

A. Rosén's group[5,6] pointed out that the profile of the OH−LIF intensity differed largely from the profile of the desorption rate, when they changed the total pressure by changing the input mass flow of the reactant. In their experiments, the reactant was supplied to the catalyst surface vertically in the stagnation point flow geometry, so the OH concentration was largely influenced by the mass transport of OH by the flow vertical to the surface. Since the reactant was supplied parallel to the surface in our experiments, the mass transport of OH vertical to the surface by the flow was negligible. The residence time of the reactant is kept more constant with a constant pumping speed than with a constant mass flow of the reactant. Therefore, we adjusted the total pressure by changing the input mass flow with a constant pumping speed.

Results

Derivation of the Absolute Concentration from the OH−LIF Signals. The quenching effect of the reactant gas should be considered when we derive the relative concentration of OH

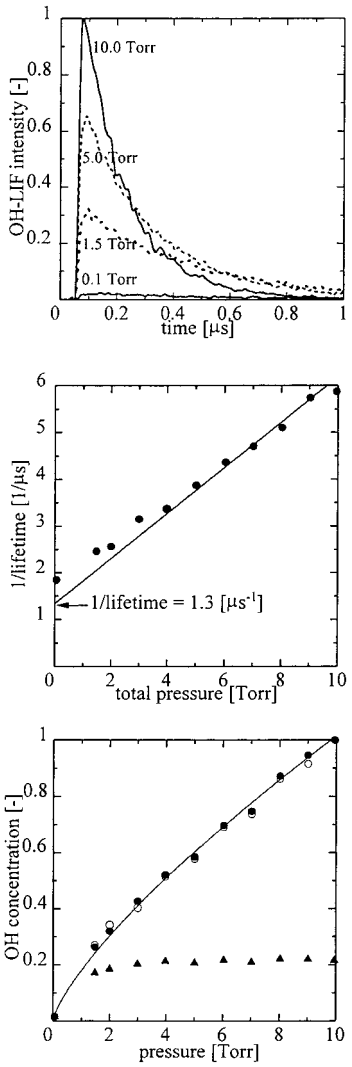

Figure 4. (a, top) Time profile of the OH−LIF signal. OH was generated in the cell shown in Figure 2 at 1200 K. (b, middle) Effect of the total pressure on the LIF lifetime at 1200 K. (c, bottom) Effect of the total pressure on the OH concentration under thermal equilibrium conditions at 1200 K.

radicals. From the work of Schofield and Steinberg,[17] the relative concentration can be expressed as[8]

$$[\mathrm{OH}]'_{\mathrm{rel}} = \frac{\sum n_{\mathrm{OH},i}}{n_{\mathrm{OH},i}} \frac{A_{ij}}{A_{ij} + \sum A_{\mathrm{im}} + k_{\mathrm{d}} + \sum k_{\mathrm{q}}[\mathrm{M_q}]} I \quad (1)$$

where $[\mathrm{OH}]'_{\mathrm{rel}}$ is the relative concentration of OH, $\sum n_{\mathrm{OH},i}$ is the total number of OH, $n_{\mathrm{OH},i}$ is the number of OH in the ith state, A_{ij} is the Einstein A coefficient for the observed emission, $\sum A_{\mathrm{im}}$ is the sum of the Einstein A coefficient for the unobserved emission, k_{d} is the rate constant for predissociation, $\sum k_{\mathrm{q}}[M_{\mathrm{q}}]$ is the sum of quenching rate constants times the concentration of the quenching agents, and I is the OH−LIF intensity normalized by the laser power. The value of $\sum n_{\mathrm{OH},i}/n_{\mathrm{OH},i}$ remains almost constant under our experimental conditions, and A_{ij} is also constant. The value of $A_{ij} + \sum A_{\mathrm{im}}$ is equal to the inverse of the lifetime ($\tau_0 = 0.75\mu$s) of OH fluorescence without quenching, which can be found in the work of J. Brzozowski et al.[16] The value of k_{d} equals zero here. So the equation is simplified to

TABLE 1: Quenching Rate Constants of OH ($A^2\Sigma^+$, $v = 1$, $N = 4$, F_1) at 1200 K (units of cm^3 molecules^{-1} s^{-1})

	this expt	in ref 8
k_{H2O}	6.2×10^{-10}	$(3.9-7.4) \times 10^{-10}$
k_{O2}	1.6×10^{-10}	$(1.1-2.2) \times 10^{-10}$
k_{Ar}	5.2×10^{-12}	
k_{He}		5.6×10^{-14}

$$[\mathrm{OH}]_{\mathrm{rel}} = \frac{I}{\frac{1}{\tau_0} + \sum k_q[\mathrm{M}_q]} \tag{2}$$

where $[OH]_{rel}$ is also the relative concentration of OH. The dominator is equal to the inverse of the LIF lifetime observed in the experiments.

Figure 4a shows the time profile of the OH−LIF signal obtained by the oscilloscope. The LIF lifetime was derived from the exponential fitting of the time profile. We obtained the relation between the lifetime and the gas composition by changing the total pressure or the partial pressure of each reactant. Figure 4b shows the effect of the total pressure on the LIF lifetime. The straight line is the result of fitting the plots with the following equation:

$$\frac{1}{\tau} = \frac{1}{\tau_0} + \frac{\sum k_q x_q}{RT} P \tag{3}$$

where τ is the observed lifetime, $k_q x_q$ is the quenching rate constant times the molar ratio of each gas, P is the total pressure, R is the gas constant, and T is temperature. The relations between the partial pressure of each gas and the lifetime were also analyzed by the following equation:

$$\frac{1}{\tau} = \frac{1}{\tau_0} + \frac{\sum_{r \neq q} k_r P_r}{RT} + \frac{k_q}{RT} P_q \tag{4}$$

where P_q and P_r are the partial pressures of gases q and r, respectively. From the results of the fitting, simultaneous equations for the quenching rate constants were obtained, and the rate constants shown in Table 1 were derived. The values agreed well with those in ref 8.

Figure 4c shows the effect of the total pressure on the relative OH concentrations. The OH−LIF signal normalized by the laser power (▲) was corrected by the procedure described above, and the relative OH concentration (●) was obtained. The relative OH concentration was also obtained by another method (○). The OH−LIF intensity is proportional to the Einstein A coefficient times the number of excited OH molecules. Since there is no quenching effect immediately after the laser excitation, the peak height normalized by the laser power in the LIF time profiles in Figure 4a is proportional to the OH concentration.

The results from both methods (● and ○) agreed well with the theoretical curve (−), proving that the relative concentrations were successfully derived. The absolute OH concentrations in other experiments can be obtained from the relation between the measurements under equilibrium and the thermodynamic calculations.

Catalytic Generation of OH over the Surfaces. Since the experiments were performed under steady-state conditions, adsorption on the surface did not change the composition of the elements in the gas phase. We calculate the gas-phase OH concentration under equilibrium conditions and compare it with the measured OH concentration in the following sections.

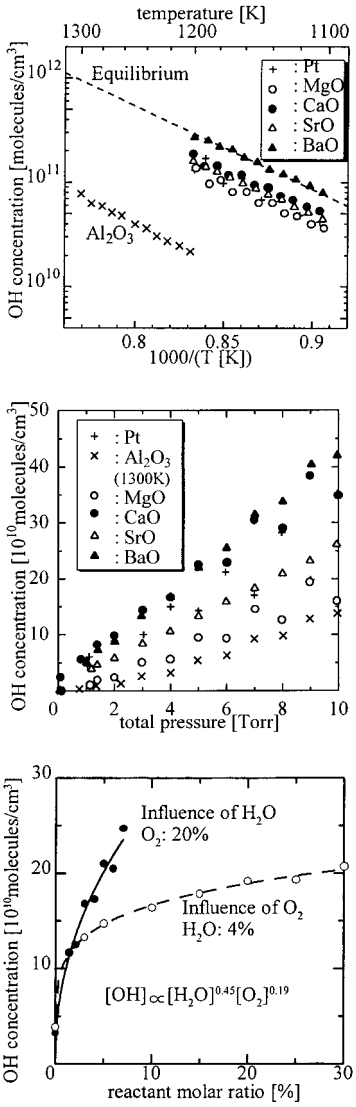

Figure 5. (a, top) Arrhenius plot of the OH concentration generated in the catalytic reaction of H_2O and O_2 at 6.0 Torr. (b, middle) Effect of the total pressure on the OH concentration generated in the catalytic reaction of H_2O and O_2 at 1200 K. The data over Al_2O_3 were obtained at 1300 K. (c, bottom) Effect of the reactant molar ratio on the OH concentration generated in the H_2O and O_2 reaction over CaO at 1200 K and 6.0 Torr.

OH Generation in the Reaction of H_2O and O_2. Figure 5a is the Arrhenius plot of the OH concentration generated in the reaction of H_2O and O_2 over the catalysts. Al_2O_3 showed the lowest catalytic activity. The OH concentration and the apparent activation energy over the other catalysts were almost the same as those under the equilibrium conditions. Figure 5b shows the effect of the total pressure on the OH concentration. The OH concentration changed almost linearly with the total pressure over all the catalysts. Figure 5c shows the effect of the molar ratios of H_2O and of O_2 on the OH generation over CaO. Both molar ratios had a positive effect on the OH generation, but H_2O had a larger effect. The other alkaline earth metal oxides had almost the same properties. Over Pt, O_2 had a smaller effect on OH concentration than the metal oxides. Over MgO, both of the gases had almost the same effect. The characteristic constants of the OH generation for each catalyst are shown in Table 2a.

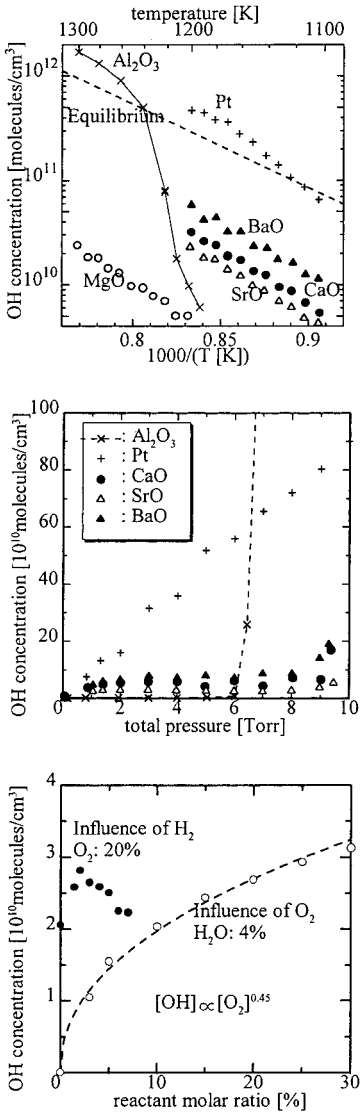

Figure 6. (a, top) Arrhenius plot of the OH concentration generated in the catalytic reaction of H_2 and O_2 at 6.0 Torr. (b, middle) Effect of the total pressure on the OH concentration generated in the catalytic reaction of H_2 and O_2 at 1200 K. (c, bottom) Effect of the reactant molar ratio on the OH concentration generated in the H_2 and O_2 reaction over CaO at 1200 K and 6.0 Torr.

OH Generation in the Reaction of H_2 and O_2. Figure 6a is the Arrhenius plot of the OH concentration generated in the hydrogen oxidation over the catalysts. The OH concentration showed the Arrhenius type dependence over all the catalysts except Al_2O_3. Pt had the highest catalytic activity, and the OH concentration exceeded the thermodynamic equilibrium value. The alkaline earth metal oxides (e.g., CaO, SrO, BaO) had the intermediate activity, and MgO had the lowest activity. As for Al_2O_3, the OH concentration changed sharply around 1220 K and exceeded that over Pt at higher temperatures. Figure 6b shows the effect of the total pressure on the OH concentration. The OH concentration changed almost linearly with pressure only over Pt. Over alkaline earth metal oxides, OH concentration was constant from 2 to 8 Torr but started to increase above 8 Torr. As for Al_2O_3, OH was hardly observed below 6 Torr but rapidly increased above 6 Torr. Figure 6c shows the effect of the molar ratios of H_2 and O_2 on the OH generation over CaO. O_2 had a positive effect on the OH generation, but there was an optimum molar ratio for H_2. The other alkaline earth metal oxides showed similar properties. Over Pt, both of the gases had a positive effect with O_2 having the larger effect. The characteristic constants of the OH generation for each catalyst are shown in Table 2b.

TABLE 2: Characteristics of OH Generation[a]

(a) In Catalytic Reaction of H_2O and O_2

	[OH][b]	E_a[c]	H_2O[d]	O_2[d]
equilibrium	29	153	0.5	0.25
Pt	15	152	0.45	0.11
Al_2O_3	2.1	167	0.37[e]	0.20[e]
MgO	13	144	0.37	0.32
CaO	17	140	0.45	0.19
SrO	16	145	0.40	0.18
BaO	28	143	0.47	0.19

(b) In Catalytic Reaction of H_2 and O_2

	[OH][b]	E_a[c]	H_2[d]	O_2[d]
equilibrium	29	153	0.5	0.25
Pt	56	238	0.13	0.54
Al_2O_3	ignition			
MgO	0.5	210		
CaO	3	198	*f*	0.41
SrO	2	194	*f*	0.49
BaO	5	182	*f*	0.47

[a] Standard experimental conditions: 1200 K, 6 Torr, 4% H_2O or H_2, 20% O_2, 76% Ar. [b] OH concentration under the conditions listed above [10^{10} molecules/cm^3]. [c] Apparent activation energy [kJ/mol]. [d] The order of OH concentration dependence on the partial pressure of each gas. [e] At 1300 K. [f] There was an optimum H_2 molar ratio for OH generation.

Estimation of the OH Generation in the Gas-Phase Reaction. To estimate the OH generation by the gas-phase reactions, a kinetic simulation using CHEMKIN[9] code was carried out. The following reactions were included in the code.

$$H_2 + O_2 = 2OH \quad \text{(I)}$$

$$OH + H_2 = H_2O + H \quad \text{(II)}$$

$$O + OH = O_2 + H \quad \text{(III)}$$

$$O + H_2 = OH + H \quad \text{(IV)}$$

$$H + O_2 + M = HO_2 + M \quad \text{(V)}$$

$$OH + HO_2 = H_2O + O_2 \quad \text{(VI)}$$

$$H + HO_2 = 2OH \quad \text{(VII)}$$

$$O + HO_2 = O_2 + OH \quad \text{(VIII)}$$

$$2OH = O + H_2O \quad \text{(IX)}$$

$$2H + M = H_2 + M \quad \text{(X)}$$

$$2H + H_2 = 2H_2 \quad \text{(XI)}$$

$$2H + H_2O = H_2 + H_2O \quad \text{(XII)}$$

$$H + OH + M = H_2O + M \quad \text{(XIII)}$$

$$H + O + M = OH + M \quad \text{(XIV)}$$

$$2O + M = O_2 + M \quad \text{(XV)}$$

$$H + HO_2 = H_2 + O_2 \quad \text{(XVI)}$$

$$2HO_2 = H_2O_2 + O_2 \quad \text{(XVII)}$$

$$H_2O_2 + M = 2OH + M \quad \text{(XVIII)}$$

$$H_2O_2 + H = HO_2 + H_2 \quad \text{(XIX)}$$

$$H_2O_2 + OH = H_2O + HO_2 \quad \text{(XX)}$$

Parts a and b of Figure 7 show the time profiles of the OH concentration in the reaction of H_2O and O_2 and in the reaction of H_2 and O_2, respectively. In the reaction of H_2O and O_2 the OH concentration increased slowly, reaching 90% of the equilibrium value after 900 s. To estimate the effect of the surface-generated OH, 1 ppm of OH was added to the initial gas composition (broken curve). The addition promoted the OH generation by 35 s, but there was no difference in shape between the two curves.

In the reaction of H_2 and O_2 the OH concentration increased rapidly, reaching the equilibrium value after a few milliseconds and 300 times that after 10 ms. The OH addition promoted OH generation for 10 ms but had little effect after 10 ms.

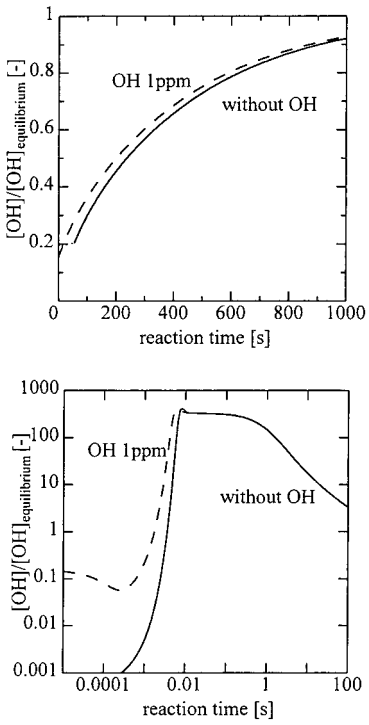

Figure 7. (a, top) Calculated results of the change of OH concentration with time generated in the gas-phase reaction of H_2O and O_2 at 1200 K and 6.0 Torr. (b, bottom) Calculated results of the change of OH concentration with time for the gas-phase reaction of H_2 and O_2 at 1200 K and 6.0 Torr.

Discussion

From the experimental results stated above, the catalysts can be classified into four groups as shown in Table 3. The following discussion of the reaction mechanism proceeds with this classification in mind.

OH Generation in the Reaction of H_2O and O_2. In the OH generation from H_2O, all the catalysts except Al_2O_3 had high catalytic activity, and the OH concentration was almost the same as the equilibrium value. The activation energy was similar to the calculated equilibrium value, and the dependence on the molar ratio of the reactants also agreed well with the equilibrium value particularly for the alkaline earth metal oxides (CaO, SrO, BaO). So we conclude that the OH generation rate was so fast that the OH concentration both on the surface and in the gas phase almost reached equilibrium within a residence time of 4 ms for all the catalysts except Al_2O_3.

OH Generation in the Reaction of H_2 and O_2. In this reaction, the catalysts showed quite different characteristics from each other. OH concentration exceeded the equilibrium concentration in the reaction over Pt. It is known that the OH desorbed from Pt can induce the gas-phase radical chain reaction through the mechanism of catalytic ignition,[1] which explains the OH concentration over Pt. For the other catalysts, the OH concentration was below the equilibrium. We discuss the reaction mechanisms next.

Rate-Determining Step of the OH Generation in the Reaction of H_2 and O_2 over Basic Metal Oxides. In this reaction, the OH generation was less than that in the reaction of H_2O and O_2, in which the OH concentration reached equilibrium. Since the inlet gases were supplied in almost the same elementary ratio in the two reactions (H/O was 2/10 and 2/11, respectively), the OH concentration should be the same in the two reactions under thermodynamic equilibrium conditions. It is clear that the OH generation did not reach equilibrium, so there exists a rate-determining step in the reaction of H_2 and O_2. In this reaction system, three steps (adsorption, surface reactions, and desorption) should be considered to determine the rate-determining step. Since the experimental results were obtained under steady-state conditions, all the steps except the rate-determining one are at equilibrium.

TABLE 3: Classification of Catalysts for OH Generation

	catalyst	$H_2 + O_2$	$H_2O + O_2$
i	Pt	high	high
ii	CaO, SrO, BaO	middle	high
iii	MgO	low	high
iv	Al_2O_3	low ignition[a]	low

[a] OH concentration rapidly increased with temperature increase by gas-phase ignition.

If the desorption was the rate-determining step, the other steps should be at equilibrium. As stated above, the inlet gases were supplied in almost the same elementary ratio as in the reaction of H_2O and O_2, and the composition of the surface species should be also the same. Since the OH desorption rate is determined only by the catalyst and the composition of the surface species, the desorption rate should also be the same. This conflicts with the experimental result, so desorption cannot be the rate-determining step. This conclusion is contrary to previous research, in which the desorption process controlled the OH generation rate over noble metals under high vacuum conditions.[5]

Next we consider adsorption. In the case of the alkaline earth metal oxides (CaO, SrO, BaO), the OH generation did not depend on the total pressure over a wide range (2−8 Torr). This typically occurs when the adsorption of the reactants reaches equilibrium at high coverage. If adsorption is the rate-determining step, the coverage should be lower and depend on the total pressure more strongly than when adsorption is at equilibrium. Thus, adsorption is probably at equilibrium, and the total reaction rate was most likely determined by surface reactions.

Mechanism of the Surface Reactions of H_2 and O_2 over Basic Metal Oxides. In the surface oxidation reactions over metal oxides, ionic species can play important roles. The adsorption of O_2 on basic metal oxides has been studied by the

ESR technique, and the reactions of surface oxygen anion species were well investigated especially on MgO at room temperature or lower temperatures.[18] Hewett et al.[8] studied the reaction of H_2O and O_2 over lanthanide metal oxides under nearly the same conditions as our experiments, and they proposed the following reaction mechanism:

$$H_2O + O_S^- \leftrightarrow OH + OH_S^- \quad (5)$$

$$2OH_S^- \leftrightarrow H_2O + \square + O_S^{2-} \quad (6)$$

$$O_2 \leftrightarrow 2O_S \quad (7)$$

$$O_S + \square + O_S^{2-} \leftrightarrow 2O_S^- \quad (8)$$

where "□" refers to an oxygen vacancy and the subscript "S" refers to a surface species.

Next, we consider the adsorption and the reactions of H_2. MgO proved to have a high catalytic activity in the H_2-D_2 exchange reaction after neutron or ultraviolet irradiation,[11,12] as well as after evacuation at high temperature.[13] MgO and the alkaline earth metal oxides were also found to show high catalytic activity for the hydrogenation of olefins after evacuation at around 1100 K.[14,15] The strong dependence of catalytic activity on the evacuation temperature indicated that the surface structures as well as the desorption of surface species were important. It is believed that H_2 heterolytically dissociates to produce H^+ and H^- ions on the O^{2-} site and Mg^{2+} site, respectively. In our experiment, the OH generation was carried out under the same conditions as in these previous studies (1100−1300 K under vacuum), so the adsorption of H_2 should proceed by the same mechanism.

H_2 and H_2O both can act as hydrogen sources in OH generation. MgO showed little activity in our experiment, so it is difficult to discuss the reaction mechanism. For the other oxides (CaO, SrO, BaO), there was an optimum concentration of H_2 for the OH generation. This phenomenon can be explained as follows.

For H_2, the following reactions are assumed.

$$H_2 \text{ dissociation:} \quad H_2 \rightarrow H_S^+ + H_S^- \quad (9)$$

$$\text{OH generation:} \quad H_S^+ + O_S^- \rightarrow OH_S \quad (10)$$

$$\text{OH consumption:} \quad H_S^- + O_S \rightarrow OH_S^- \quad (11)$$

$$H_S^+ + O_S^{2-} \rightarrow OH_S^- \quad (12)$$

followed by

$$OH_S^- + OH \rightarrow H_2O + O_S^- \quad (5')$$

At low H_2 pressure, an increase in the molar ratio of H_2 has a positive effect on the OH generation by accelerating reaction 10. However, at high H_2 pressure, reaction 11 or 12 can be important, resulting in the consumption of surface OH by reaction 5′.

OH generation from H_2O is considered to proceed by reactions 5−8. At low H_2 pressure, H_2 contributes positively to the generation of H_2O, and therefore, the OH generation is promoted by reaction 5. At high H_2 pressure, inhibition of reaction 5 by the direct reaction of H_2 with O^- could become important, and this reaction would lead to the suppression of OH generation.

From the discussion above, both routes for the OH generation seem to be possible. The dominant route cannot be determined, however, because the OH generation from the reaction of H_2 and O_2 is always accompanied by the generation of H_2O.

Effect of the MgO and Al_2O_3 Surfaces on the Gas-Phase Ignition. Both MgO and Al_2O_3 had little catalytic activity in the reaction of H_2 and O_2 below 1200 K, but they showed quite different behaviors at higher temperatures. The OH concentration over MgO remained low but that over Al_2O_3 increased rapidly with a temperature increase. A rapid increase of OH over Al_2O_3 was also observed with a total pressure increase. The surface reaction mechanism can hardly explain these discontinuities. Since these phenomena typically appear in the gas-phase chain reaction, we concluded that the reaction conditions were close to the limit of inflammability and that gas-phase ignition occurred. The difference between MgO and Al_2O_3 can be explained by the consumption rate of OH on the surface as follows. Above 1200 K, OH is produced by the gas-phase reaction of H_2 and O_2. The produced OH diffuses to the solid surface when the OH concentration near the surface is low. Since the reversible reaction of H_2O and O_2 to form OH is fast on the MgO surface, the sticking coefficient of OH on MgO is large. OH adsorbs on the surface and is consumed rapidly through recombination or reaction with surface species (H_2 or H ions), so the gas-phase ignition is suppressed. Al_2O_3 has so little OH generation activity that OH is hardly consumed on its surface, and the gas-phase ignition occurs. Hence, the consumption rate of OH on the surface may be one of the factors controlling the gas-phase ignition.

Conclusions

Basic metal oxides proved to be good catalysts for rapid OH generation from water but not for the OH generation from hydrogen.

In the OH generation from H_2O and O_2, basic metal oxides (MgO, CaO, SrO, BaO) showed high catalytic activity, and the OH concentration over the oxides almost reached the thermodynamic equilibrium value within a residence time of 4 ms.

In the OH generation from H_2 and O_2, the alkaline earth metal oxides (CaO, SrO, BaO) showed catalytic activities that were less than that of Pt. The other oxides (MgO and Al_2O_3) showed the lowest activities. The rate-determining step for OH generation over the alkaline earth metal oxides was probably the surface reaction process under our experimental conditions. The OH concentration showed a large change with changes in temperature or pressure only over Al_2O_3. This phenomenon was attributed to gas-phase ignition, and the consumption rate of OH at the surface is proposed to be one of the factors controlling this process.

Acknowledgment. We thank professor Mitsuo Koshi of the University of Tokyo for his kind advice regarding the LIF measurement and the computer calculations. We also thank Dr. Toshihide Baba of Tokyo Institute of Technology and Dr. Takehiko Sasaki of the University of Tokyo for their fruitful comments on the surface reaction mechanisms. Moreover we thank professor Tatsuya Okubo of the University of Tokyo for his advice on our overall research.

References and Notes

(1) Pfefferle, L. D.; Griffin, T. A.; Winter, M.; Crosley, D. R.; Dyer, M. J. *Combust. Flame* **1989**, *76*, 325.

(2) Ljungström, S.; Hall, J.; Kasemo, B.; Rosén, A.; Wahnström, T. *J. Catal.* **1987**, *107*, 548.

(3) Hsu, D. S. Y.; Hoffbauer, M A.; Lin, M. C. *Surf. Sci.* **1987**, *184*, 25.
(4) Williams, W. R.; Marks, C. M.; Schmidt, L. D. *J. Phys. Chem.* **1992**, *96*, 5922.
(5) Gudmundson, F.; Fridell, E.; Rosén, A.; Kasemo, B. *J. Phys. Chem.* **1993**, *97*, 12828.
(6) Fridell, E.; Rosén, A.; Kasemo, B. *Langmuir* **1994**, *10*, 699.
(7) Anderson, L. C.; Xu, M.; Mooney, C. E.; Rosynek, M. P.; Lunsford, J. H. *J. Am. Chem. Soc.* **1993**, *115*, 6322.
(8) Hewett, K. B.; Anderson, L. C.; Rosynek, M. P.; Lunsford, J. H. *J. Am. Chem. Soc.* **1996**, *118*, 6992.
(9) Gordon, S.; McBride, B. J. Report NASA SP-273; NASA: Washington, DC, 1971.
(10) Kee, Robert J.; Rupley, F. M.; Miller, J. A. Sandia National Laboratories Report SAND89-8009; Sandia National Laboratories: Albuquerque, NM, 1989.
(11) Lunsford, J. H.; Leland, T. W. *J. Phys. Chem.* **1962**, *66*, 2591.
(12) Lunsford, J. H. *J. Phys. Chem.* **1964**, *68*, 2312.
(13) Boudart, M.; Delbouille, A.; Derouane, E. G.; Indovina, V.; Walters, A. B. *J. Am. Chem. Soc.* **1972**, *94*, 6622.
(14) Tanaka, Y.; Hattori, H.; Tanabe, K. *Chem. Lett.* **1976**, 37.
(15) Hattori, H.; Tanaka, Y.; Tanabe, K. *Chem. Lett.* **1975**, 659.
(16) Brzozowski, J.; Erman, P.; Lyyra, M. *Phys. Scr.* **1978**, *17*, 507.
(17) Schofield, K.; Steinberg, M. *Opt. Eng.* **1981**, *20*, 501.
(18) Lunsford, J. H. *CRC Crit. Rev. Solid State Sci.* **1976**, *6*, 337.